Smart Mater. Struct. 3 (1994) 476–484. Printed in the UK

Active control of far-field sound radiation by a beam with piezoelectric control transducers: Physical system analysis*

Bor-Tsuen Wang

Department of Mechanical Engineering, National Pingtung Polytechnic Institute, Pingtung, Taiwan 91207, Republic of China

Received 18 January 1994, accepted for publication 20 July 1994

Abstract. This paper analytically demonstrates the use of piezoelectric actuators and PVDF sensors to actively control the far-field sound radiation from a simply-supported beam in an infinite rigid baffle. The beam is assumed to be subjected to a harmonic point force. The piezoelectric patches which are attached to the beam serve as actuators to control the sound radiated from the beam into the far-field, while the PVDF films serve as structural error sensors. A minimization process is used to calculate the optimal input voltages into the piezoelectric actuators so as to minimize the cost function which is the least mean square value of the error sensor signals. Radiation directivity patterns are plotted, and the wavenumber analysis is performed to evaluate the control effectiveness. Results show that the use of the compact distributed types of actuators and sensors can efficiently attenuate the far-field sound radiation. The reduction of sound pressure level for on-resonance cases is over 20–50 dB; however, little attenuation can be achieved or even spillover may occur for off-resonance cases due to the arbitrary location of actuators and sensors. This work demonstrates the use of structural actuators and near-field sensors for far-field sound radiation control and leads to the inherent application of an intelligent material structure system.

1. Introduction

Active structural acoustic control (ASAC) have been drawn a great deal of interest over the past few years. Leug [1] first proposed cancelling the primary sound wave with the use of a secondary sound wave 180° out-of-phase with respect to the primary source. The sound source (speaker) which is not a 'real' actuator is to applied in the acoustic field to cancel the sound wave. Many researchers have shown the feasibility of sound sources in active noise control (ANC) [2–5]. Another effective way to control the structural sound radiation is to apply control force directly to the radiated structures. Shakers can efficiently control the sound radiation [6–8] although they have substantial disadvantages due to their large volume, large weight and support requirements. Recently, the compact distributed types of actuators, such as piezoelectric patches, have been shown to be feasible for structural vibration and acoustic control [9–12].

Microphones are generally used as error sensors in ASAC; however, the fact that microphones must be located in the radiated far-field makes them impractical for applications. Structural sensors, such as accelerometers, have been proposed for ASAC [13]. Although accelerometers overcome the disadvantages of far-field sensors, they are still impractical for implementation due to the high cost and the difficulty of adherence to the structure. PVDF sensors, which are film type sensors attached to the structure, have been applied to structural vibration and acoustic control [14, 15]. The PVDF sensors are more practical than microphones or accelerometers for applications because of their compactness and low cost.

Structural sound radiation control can be achieved by either modifying the dynamic response of the structure or influencing the structure associated acoustic response. Both the vibration-based error sensor and the acoustic-field error sensor can be implemented into the active control system. One may construct their corresponding cost functions, such as the structural kinetic energy and the radiated acoustic power [16–18]. The cost functions can then be minimized to perform efficient control of

* Partial results of the paper was presented at the tenth National Conference of the Chinese Society of Mechanical Engineers, Hsinchu, Taiwan, Republic of China, December, 1993.

0964-1726/94/040476+09$19.50 © 1994 IOP Publishing Ltd

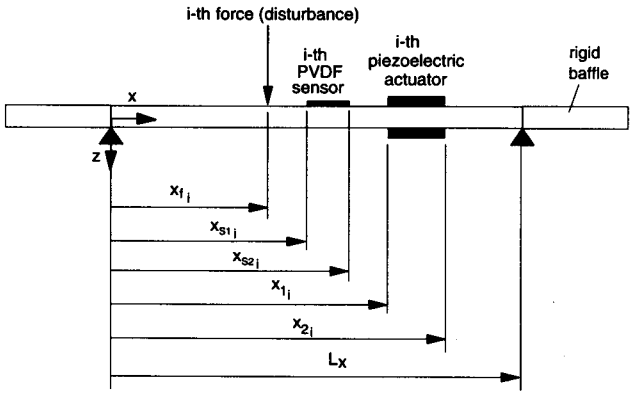

Figure 1. The arrangement and coordinates of a simply-supported beam.

structural sound radiation.

This paper presents the use of compact distributed piezoelectric actuators and PVDF film sensors for active control of far-field sound radiation from a beam. The simply-supported beam mounted in an infinite rigid baffle subjected to a harmonically excited point force is considered as the plant. Both piezoelectric actuators and PVDF sensors are attached to the radiated structure. A linear quadratic optimization process is applied to obtain the optimal control voltages input to the piezoelectric actuators so as to minimize the cost function. The cost function is constructed as the sum of the least mean square value (LMS) of error sensor signals. The structural response and sound radiation directivity pattern were studied to show the control effectiveness as well as the wavenumber analysis. Results show that sufficient control can be achieved for on-resonance cases. Little reduction of sound pressure level or even spillover may occur for off-resonance cases due to the inappropriate location of sensors and actuators. The optimization of the design of actuators and sensors may require further study. Nevertheless, this work shows the effectiveness of far-field sound radiation with the use of near-field structural actuators and sensors. This work also leads to an inherent application of intelligent material structures, which can integrate actuators and sensors into the structures, to the ASAC.

2. Theoretical analysis

2.1. Lateral vibration of uniform beam

Consider a uniform simply-supported beam with length of L, as shown in figure 1. The equation of motion can be obtained as follows:

$$E_b I \frac{\partial^2 w}{\partial x^4} + \rho_b b t \frac{\partial^2 w}{\partial t^2} = p(x, t) \tag{1}$$

where E_b is the Young's modulus of the beam; I is the moment of inertia; ρ_b is the beam density; t_b is the beam thickness; b is the beam width; and $p(x, t)$ is the force function. Note that the damping effect is assumed small and can be neglected. The boundary conditions for a simply-supported beam are

$$M(0, t) = M(L, t) = E_b I \frac{\delta^2 w}{\delta x^2} = 0 \tag{2}$$

$$w(0, t) = w(L, t) = 0. \tag{3}$$

For free vibration analysis, i.e. $p(x, t) = 0$, the natural frequencies can be found to be

$$\omega_n = (n\pi)^2 \sqrt{\frac{E_b I}{\rho_b b t_b L^4}}. \tag{4}$$

The general form of beam lateral displacement, while the beam is subjected to harmonic force inputs, can be written as follows:

$$w(x, t) = e^{i\omega t} \sum_{n=1}^{\infty} W_n \sin \alpha_n x \tag{5}$$

where

$$\alpha_n = \frac{n\pi}{L} \tag{6}$$

$$W_n = \frac{P_n}{\rho_b b t_b (\omega_n^2 - \omega^2)}. \tag{7}$$

Here ω is the excitation frequency; α_n is the modal number; W_n is the modal amplitude; and P_n is the modal force depending on the forms of external forces.

2.1.1. Point force excitation. For a harmonic point force with the amplitude F located at x_f acting on the beam, the force function, $p(x, t)$, can be written as follows:

$$p(x, t) = F\delta(x - x_f)e^{i\omega t}. \tag{8}$$

The delta function, $\delta(x)$, is employed to represent the location of the point force. The modal force, P_n^f, due to the point force excitation is given as follows:

$$P_n^f = \frac{2F}{L} \sin \alpha_n x_f \tag{9}$$

where the superscript f signifies the point force.

2.1.2. Piezoelectric excitation. For an actuator consisting of two identical piezoceramic patches bonded symmetrically on the two opposite beam surfaces and activated 180° out-of-phase, the equivalent external forces can be derived as follows [19]:

$$p(x, t) = M_{eq}[\delta'(x - x_1) - \delta'(x - x_2)]e^{i\omega t} \tag{10}$$

where

$$M_{eq} = C_0 \Delta = \frac{t_b^2 E_b}{6} K b_a \Delta \tag{11}$$

$$K = \frac{6}{6 + \Psi} \tag{12}$$

$$\Psi = \frac{E_b t_b}{E_a t_a} \tag{13}$$

$$\Delta = \frac{d_{31}}{t_a} V \tag{14}$$

$C_0\Delta$ is the equivalent moment induced by the piezoelectric patches attached to the top and bottom of the beam and excited 180° out-of-phase. Δ is the strain induced by an unconstrained piezoelectric layer of thickness t_a, when a voltage V is applied along its polarization direction, while d_{31} is the piezoelectric strain coefficient. Ψ is the effective stiffness ratio. t_a and E_a are the thickness and Young's modulus of the piezoelectric patch respectively. The resultant force is, in fact, the concentrated moments acting on both edges of the piezoelectric patches represented by the first derivative of the delta function. The corresponding expression of modal force for piezoelectric excitation, P_n^c, can be derived [19] as follows:

$$P_n^c = \frac{2M_{eq}}{L}\alpha_n\left(\cos\alpha_n x_1 - \cos\alpha_n x_2\right) \tag{15}$$

where x_1 and x_2 are the coordinates of the piezoelectric actuator, and the superscript c signify the control force.

2.2. PVDF sensor equation

For a PVDF film arranged as shown in figure 1, the shape function can be expressed as follows:

$$\Gamma(x) = u\left(x - x_{s1}\right) - u\left(x - x_{s2}\right) \tag{16}$$

where $u(x)$ is the step function; x_{s1} and x_{s2} are the coordinates of the PVDF film. The sensor equation can then be derived as follows [20]:

$$q(t) = \frac{t_b + t_s}{2} b_s e_{31} \int_0^L \Gamma(x)\frac{\partial^2 q}{\partial x^2}\,\mathrm{d}x \tag{17}$$

where b_s is the sensor width; t_s is the sensor thickness; and e_{31} is the piezoelectric field intensity constant. By substituting and integrating over the beam length,

$$q(t) = \mathrm{e}^{\mathrm{i}\omega t}\left(\frac{t_b + t_s}{2} e_{31}\right)\sum_{n=1}^{\infty}\alpha_n W_n \times \left(\cos\alpha_n x_{s2} - \cos\alpha_n x_{s1}\right). \tag{18}$$

The generated voltages can then be expressed as:

$$V(t) = \frac{q(t)}{\epsilon A} t_s \tag{19}$$

where ϵ is the permittivity of PVDF films; and A is the sensor area. It is noted that the generated voltage is proportional to the slope difference of the beam between the two edges of the PVDF film location.

2.3. Sound radiated into the far-field

The far-field sound pressure radiated from a vibrating surface at a point in the acoustic field, as shown in figure 2, is given by the Rayleigh integral [21]:

$$p(\boldsymbol{r}, t) = \frac{\mathrm{i}\omega\rho}{2\pi}\int_s \dot{w}(\boldsymbol{r}_s)\frac{\mathrm{e}^{-\mathrm{i}\kappa R}}{R}\,\mathrm{d}s \tag{20}$$

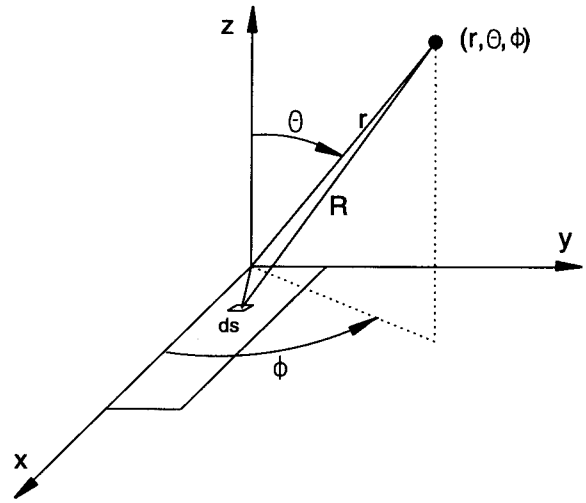

Figure 2. Sound radiated coordinate system.

where $\boldsymbol{r}$ is the position vector of the observation point; $\boldsymbol{r}_s$ is the position vector of the elemental surface; ds; $\dot{w}(\boldsymbol{r}_s)$ is the normal velocity of ds; R is $|\boldsymbol{r} - \boldsymbol{r}_s|$; ρ is the fluid density; and $\kappa = \omega/c$ is the acoustic wavenumber. Here, the acoustic medium is air, and thus there is no feedback of the fluid motion into the structure. By substituting the beam velocity derived from equation (5) into the Rayleigh integral, the sound pressure radiated to the far-field can be obtained [22]:

$$p(r, \theta, \phi\, t) = \mathrm{e}^{\mathrm{i}\omega t}\sum_{n=1}^{\infty} W_n q_n \tag{21}$$

where

$$q_n = -\mathrm{i}\omega\frac{\rho c b}{\pi}\frac{\kappa}{\alpha_n}\frac{\mathrm{e}^{-\mathrm{i}\kappa r}}{2r}\left[\frac{1 - (-1)^n\mathrm{e}^{-\mathrm{i}\alpha}}{1 + (\alpha/n\pi)^2}\right]\left[\frac{1 - \mathrm{e}^{-\mathrm{i}\beta}}{\beta}\right] \tag{22}$$

$$\alpha = \kappa L \sin\theta\cos\phi \tag{23}$$

$$\beta = \kappa b \sin\theta\sin\phi. \tag{24}$$

Under the assumption of superposition, the total radiated sound pressure can be the sum of sound pressures due to the disturbance and control inputs

$$p_t = p_f + p_c = \mathrm{e}^{\mathrm{i}\omega t}\sum_{n=1}^{\infty}\left(W_n^{\mathrm{f}} + W_n^c\right)q_n. \tag{25}$$

The total radiated sound power defined as the integral of the square of the radiated sound pressure over the hemisphere of the radiating field can then be obtained:

$$\Phi_p = \frac{1}{2\rho c}\int_S |p_t|^2\,\mathrm{d}S = \frac{r^2}{2\rho c}\int_0^{2\pi}\int_0^{\pi/2}|p_t|^2\sin\theta\,\mathrm{d}\theta\,\mathrm{d}\phi. \tag{26}$$

The total radiated sound power can be an index to evaluate the effectiveness of sound radiation control.

2.4. Wavenumber analysis

The beam velocity distribution can be taken as a Fourier integral transform in κ-plane.

$$\tilde{V}(\kappa_x, \kappa_y) = \int_{-\infty}^{\infty}\int_{-\infty}^{\infty} \dot{w}(x)e^{-i(\kappa_x x+\kappa_y y)}\,dxdy \qquad (27)$$

where

$$\kappa_x = \kappa \sin\theta\cos\phi \qquad (28)$$

$$\kappa_y = \kappa \sin\theta\sin\phi \qquad (29)$$

therefore, the velocity transform can be expressed as:

$$\tilde{V}(\kappa_x, \kappa_y) = i\omega\sum_{n=1}^{\infty} W_n V_n \qquad (30)$$

where

$$V_n = i\alpha\left[\frac{1-(-1)^n e^{-i\kappa_x L}}{\alpha_n^2-\kappa_x^2}\right]\left[\frac{e^{-i\kappa_y b}-1}{\kappa_y}\right]. \qquad (31)$$

It is noted that the LMS value of the velocity transform, i.e. $|\tilde{V}|^2$, is proportional to the radiated sound power [21]. Only the wavenumber components satisfying $\kappa_x^2 + \kappa_y^2 < \kappa^2$ contribute to sound radiation into the far-field and are termed supersonic waves. Others wavenumber components do not radiate into the far-field and are termed subsonic waves.

2.5. Cost function for PVDF sensors

For N_s PVDF sensors, the cost function can be defined as the sum of the mean square voltages measured from the PVDF films:

$$\Psi_v = \sum_{j=1}^{N_s} |V_j|^2. \qquad (32)$$

The linear quadratic optimization process, which simulates the LMS feedforward control algorithm can then be applied to minimize the cost function so as to find the optimal control voltages input to the piezoelectric actuators. The full analysis can be referred to in [23] and is omitted here for brevity. The vibrating energy of the beam can also be expressed as follows:

$$\Phi_w = \int_0^L |\ddot{w}|^2\,dx \qquad (33)$$

which can be used as an index to evaluate the effectiveness of vibration control.

Table 1. Natural frequencies of the simply-supported beam.

mode	frequency (Hz)
1	33.2
2	128.8
3	289.9
4	515.4
5	805.3
6	1159.6
7	1578.3
8	2061.4
9	2609.0
10	3220.9

Table 2. Physical properties of the G-1195 piezoceramic patch [24].

$E_a = 6.3 \times 10^{10}$ N m^{-2}	$\rho_a = 7650$ Kg m^{-3}
$t_a = 1.905$ mm	$\nu_a = 0.28$
$d_{31} = d_{32} = 166 \times 10^{-12}$ m V^{-1}	

Table 3. Physical properties of the PVDF films (LDT-28μk) [25].

$E_s = 2 \times 10^9$ N m^{-2}	$\rho_s = 1800$ Kg m^{-3}
$t_s = 28 \times 10^{-6}$ m	$\nu_s = 0.33$
$e_{31} = 54 \times 10^{-3}$ C m^{-1}	$\epsilon = 106 \times 10^{-12}$ F m^{-1}

3. Numerical results and discussions

A steel beam with length 0.38 m, width 0.04 m, and thickness 2 mm is used in the simulations. The first ten natural frequencies are tabulated in table 1. It is noted that no damping was included in the following analysis. The optimal process is suitable for controlling multiple primary sources; however, only one harmonic point force with input parameters, F=0.3 N and =0.067 m, was considered for the following analysis. The physical properties of the piezoelectric patch (G-1195) [24] and PVDF films (LDT-28μk) [25] are respectively shown in tables 2 and 3. The piezoceramic patch was located at $x_1 = 0.285$ m, $x_2 = 0.3485$ m, i.e. the central location of the piezoceramic patch was right on the maximum amplitude of the third mode shape of the simply-supported beam. The PVDF film was arbitrarily selected to be located at $x_{s1} = 0.10$ m, $x_{s2} = 0.14$ m, and away from the nodal points of the first few modes. In order to calculate the beam response and radiated sound pressure, it was necessary to truncate the modal sums in equation (5). Upon consideration of computing time and accuracy, the first ten modes were considered, and it was found to provide sufficient convergence of series.

Both the radiation directivity and beam displacement distributions were shown to demonstrate the control effectiveness of sound radiation through the beam. The radiated sound pressure was plotted in dB re 20×10^{-6} Pa over $\theta = -90°$ to $90°$ at a radial distance of 3 m

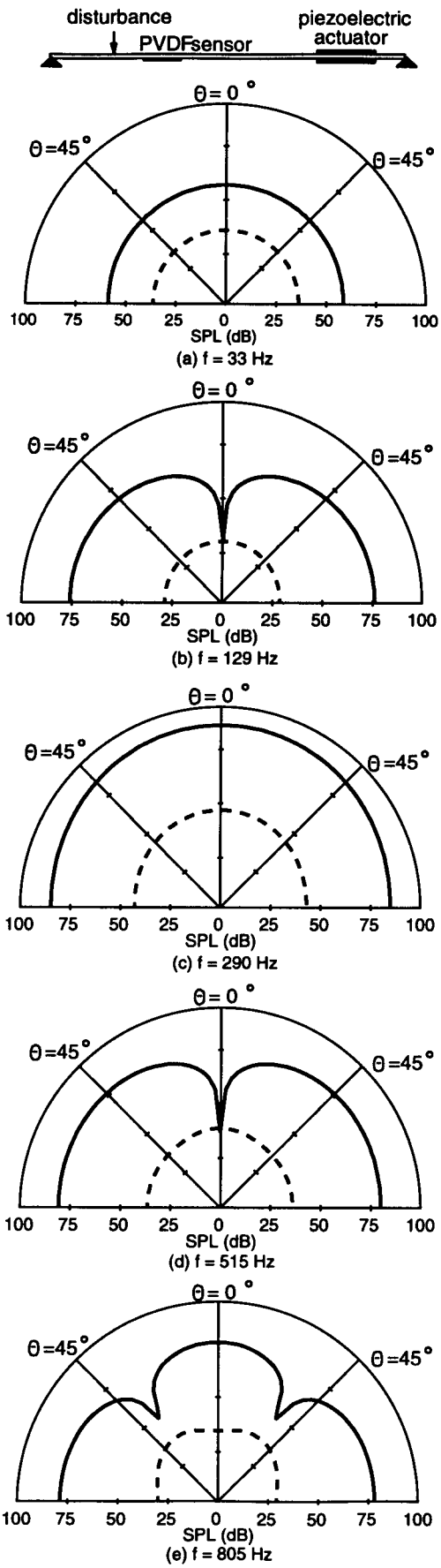

Figure 3. Radiation directivity pattern for (*a*) first, (*b*) second, (*c*) third, (*d*) fourth, and (*e*) fifth mode excitation: —— uncontrolled, - - - - controlled.

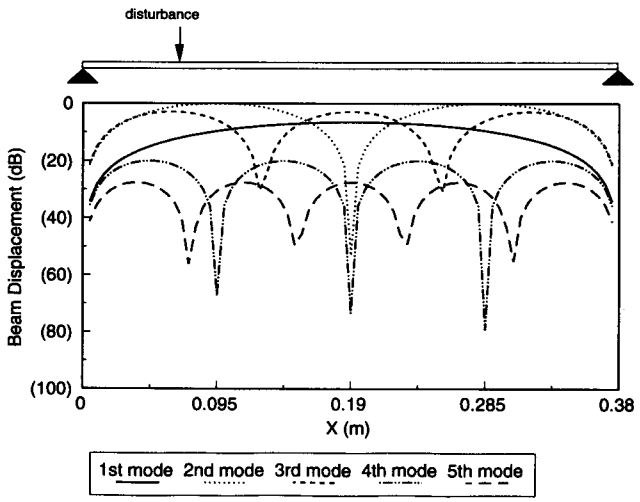

Figure 4. Uncontrolled displacement distributions for on-resonance excitation.

from the beam, which was well into the far-field. The beam displacement distribution was normalized by the largest amplitude in each case and plotted in logarithmic scale (dB) along the beam length.

Figure 3 shows the radiation directivity for the first five resonance mode excitation cases. The arrangement of the actuator and sensor is depicted at the top of the figure. The solid line indicates the uncontrolled response. As shown in figure 3(*a*), the directivity pattern is uniform for the first mode excitation due to the disturbance, while the directivity pattern appears to dip at $\theta = 0°$ for the second mode excitation as shown in figure 3(*b*). For the third mode excitation case, the radiation directivity pattern appears like a monopole response, not as the response of the third radiation mode; however, the fact that the directivity is not uniform evidences the existence of the third mode. Also, the fifth structure mode excitation results in response like a third radiation mode as shown in figure 3(*e*). These 'reduced mode' radiation characteristics, i.e. the excitation of higher structure modes resulting in the acoustic response of lower radiation modes, can be explained by the wavenumber analysis. The controlled directivity pattern is denoted by the dashed line. A global reduction of sound pressure level over 20–50 dB can be observed for all of the on-resonance excitation cases. The residual radiation directivity pattern appears to be a lower mode shape. This indicates that the significant radiated mode is effectively controlled leaving the insignificant modal response.

The beam displacement distributions due to the disturbance for the first five resonance mode excitation cases are shown in figure 4. The second mode excitation gives the highest response because of the location of the point force disturbance. As seen in figure 4, the third mode structural response is smaller than the second mode structural response; however, the radiated sound pressure level for the third mode excitation case is higher than that for the second mode excitation case, as shown in figures 3(*b*) and 3(*c*). It is because the odd mode is the more efficient radiator than the even

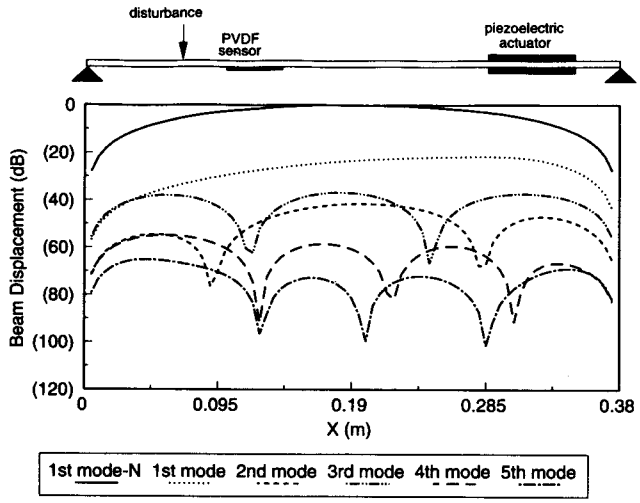

Figure 5. Controlled displacement distributions for on-resonance excitation.

mode. This can be further explained by the wavenumber analysis. The controlled beam displacement distributions for on-resonance excitation corresponding to the cases in figure 3 are shown in figure 5 for comparison. The residual beam response is found to be globally reduced for each case and to become a lower modal response. This results in the attenuation of sound radiation.

To further examine the radiation characteristics of the beam, a wavenumber analysis as shown previously is performed. The LMS value of velocity transform plotted over the structural wavenumber (κ_x) is shown in figure 6 for the on-resonance excitation cases when $\kappa_y = 0$, and the acoustic wavenumber ($\kappa = \omega/c$) is also indicated. The wavenumber components satisfying $-\kappa < \kappa_x < \kappa$ which contribute to the far-field sound radiation are characterized as the supersonic region [21]. Other wavenumber components, i.e. $|\kappa_x| > \kappa$, which do not radiate are termed the subsonic region. For odd-mode excitation, the fact that the LMS value of the velocity transform appears a peak at $\kappa_x = 0$ makes the structure an efficient radiator. Conversely, for even mode excitation a dip at $\kappa_x = 0$ makes the structure an inefficient radiator. One can also observe that the shape of the radiation directivity shown in figure 3 is related to the velocity transform in figure 6. The radiation mode shape appears in the directivity pattern exactly the same as the number of modes involved in the supersonic region. This explains the 'reduced mode' radiation characteristics mentioned previously. As control is applied, the LMS value of velocity transform is globally reduced over the wide range of the structural wavenumber. In particular, the reduction of the LMS value of velocity transform in the supersonic region implies the reduction of radiated power as mentioned previously.

Table 4 summarizes the results of on-resonance excitation cases. Φ_p which is the total radiated sound power of the beam can be an index for evaluating the effectiveness of sound radiation control, while Φ_w which is the vibrating energy can be an index for evaluating the effectiveness of vibration control [23]. The large

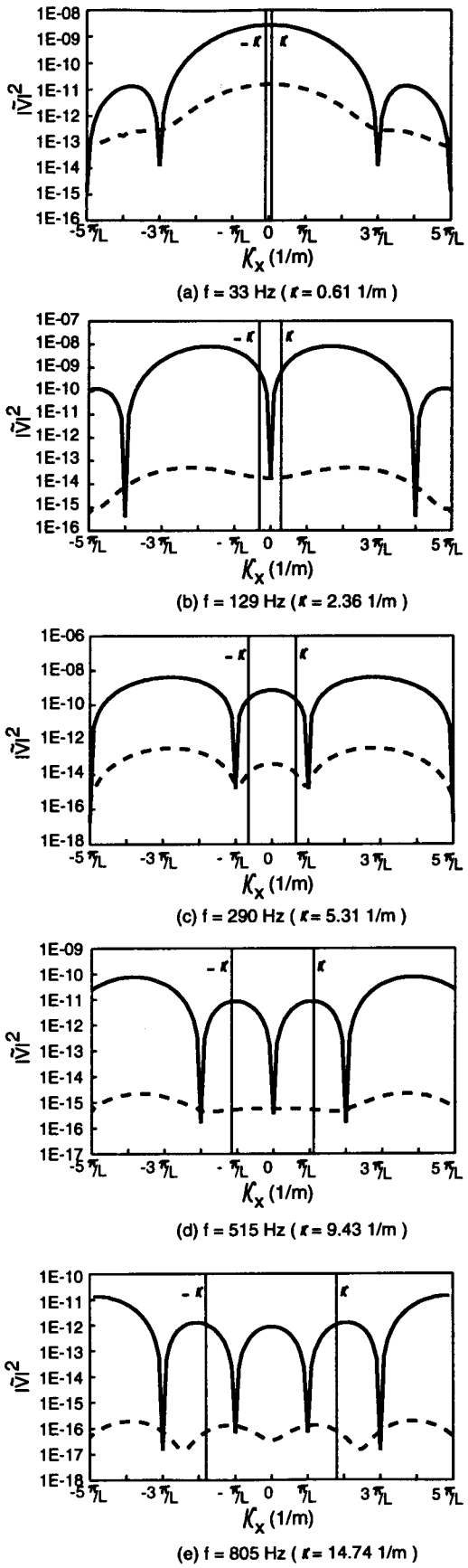

Figure 6. LMS value of velocity transform for (*a*) first, (*b*) second, (*c*) third, (*d*) fourth, and (*e*) fifth mode excitation: —— uncontrolled, ---- controlled.

Table 4. Results for the on-resonance excitation cases.

Excitation frequency (Hz)	Reduction of Φ_w (dB)	Reduction of Φ_p (dB)	Control voltages (V)
33	22.1	22.3	−94.7
129	50.5	39.1	26.4
290	40.9	42.27	−12.0
515	44.2	38.4	6.9
805	47.2	43.2	− 3.9

amount of reduction of Φ_w does not imply the equivalent amount of reduction of Φ_p. The amount of radiated sound power depends on the structural mode shape as well as the edge effect [26]. Here, the simply-supported boundary condition is considered. It is worth mentioning that for the second mode excitation case with control, the reduction of Φ_w is up to 50.5 dB; however, the reduction of Φ_p is only about 39.1 dB. It is because the residual beam response, as shown in figure 5, appears like the third mode shape which is an efficient radiator. The control voltages applied to the actuators for each case are also listed in table 4. More control effort is required for lower mode excitation, such as the case of 33 Hz near the first mode excitation requiring over 90 V. Clark *et al* [27] have experimentally shown the dynamic linearity of the piezoelectric excitation. The structural response is linear when the actuator is applied from 30 to 90 V rms ranges. A 530 V rms ranges in terms of frequency response function, and a 5range between 90 and 150 V rms.

Figure 7 shows the radiation directivity for off-resonance excitation cases. One can observe that little reduction of sound pressure level is achieved or even spillover occurs. This can be because of the inappropriate position of the actuator and sensor. The uncontrolled and controlled beam displacement distributions for off-resonance excitation cases are shown in Figures 8 and 9 respectively. The beam response is not reduced as control is applied, and the shape of radiation directivity corresponding to the structural response of the beam. The wavenumber analysis for the off-resonance excitation cases is shown in figure 10. The wavenumber components in the supersonic region are not reduced. In particular, as shown in figure 10(*b*) for $f = 210$ Hz, some wavenumber components are attenuated; however, there is more spillover in the supersonic region. As shown in table 5, the negative value of the reduction of Φ_p indicates that the radiated sound power increases after applying control; therefore, the control is ineffective. To cure the control defect of the off-resonance excitation case, the appropriate number and location of actuators and sensors must be selected; however, the optimal placement of actuators and sensors is out of the scope of this paper. The optimization problem regarding the placement of actuators and sensors was previously studied by a conventional gradient search method [28, 29], and is also currently being investigated with the use of genetic algorithms at the National Pingtung Polytechnic Institute. An alternative solution may also construct an efficient cost function, such as the LMS value of the velocity transform based on the PVDF film sensors, so as to achieve sufficient control for off-resonance excitation cases.

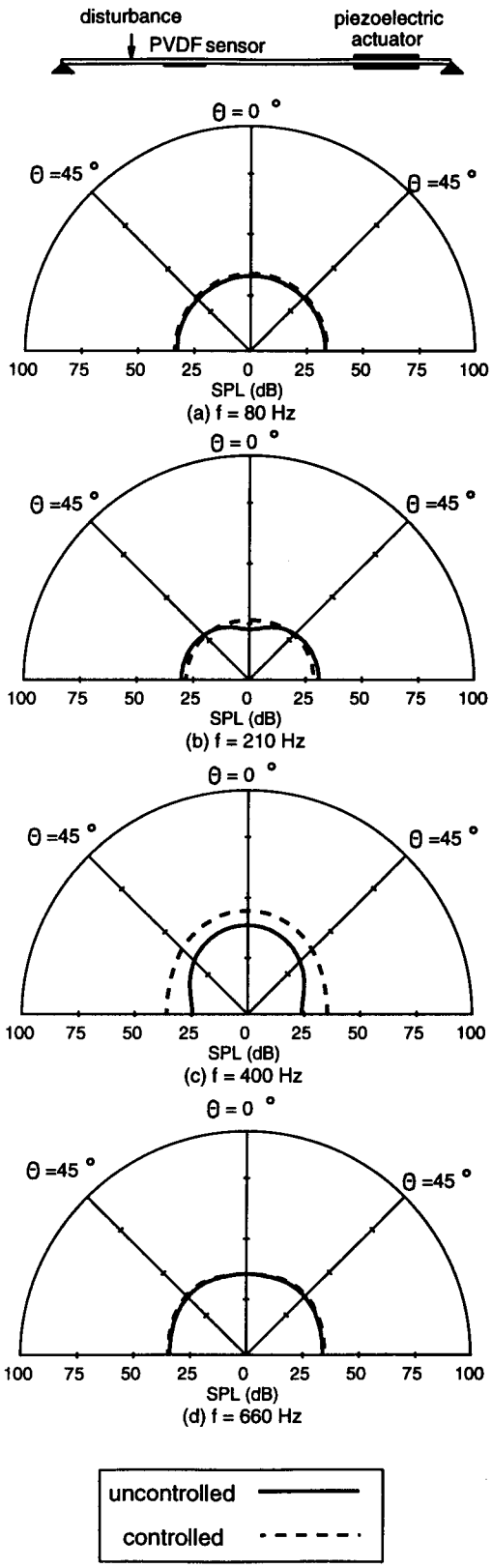

Figure 7. Radiation directivity pattern for off-resonance excitation.

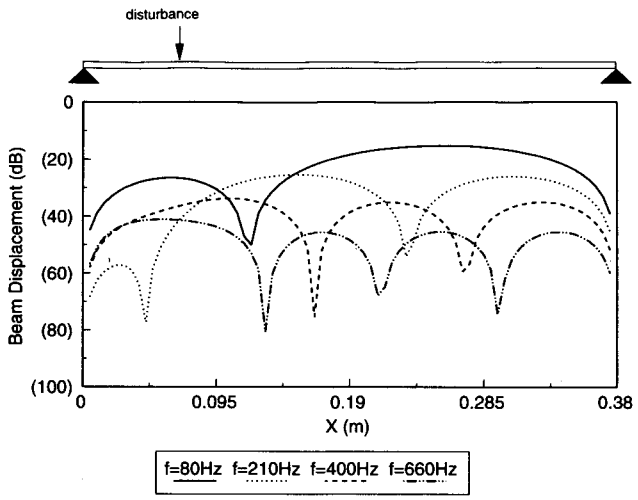

Figure 8. Uncontrolled displacement distributions for off-resonance excitation.

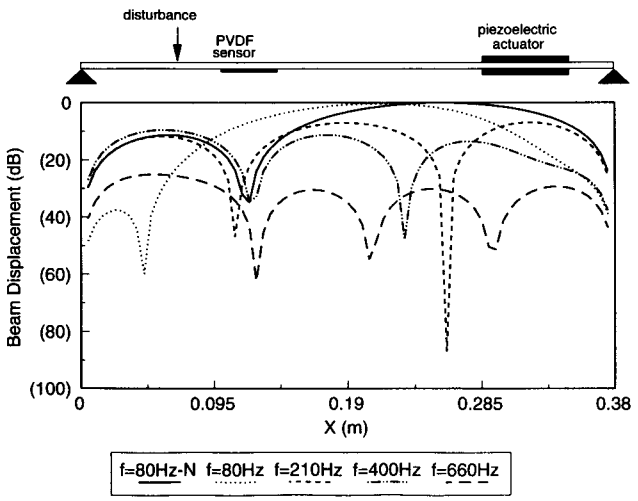

Figure 9. Controlled displacement distributions for off-resonance excitation.

4. Conclusions

This paper demonstrates the application of piezoelectric actuators and PVDF sensors to active structural acoustic control in conjunction with the use of the LMS feedforward control. Results show that PVDF film is a suitable near-field structural sensor for the ASAC in the replacement of the traditional far-field microphone error sensor. In particular, the effective control can be achieved for on-resonance excitation cases, and the radiated sound power can be attenuated over 20–40 dB. The radiation directivity and the beam displacement distribution were presented to show the characteristics of active sound radiation control. An extensive wavenumber analysis was also performed and shown to be an effective means of studying the sound radiation control mechanism. For off-resonance excitation cases, little control can be achieved or even spillover occurs due to the improper location of the actuator and sensor; therefore, a future study on the optimal placement of piezoelectric actuators and PVDF sensors may be needed in order to achieve sufficient control. The alternative

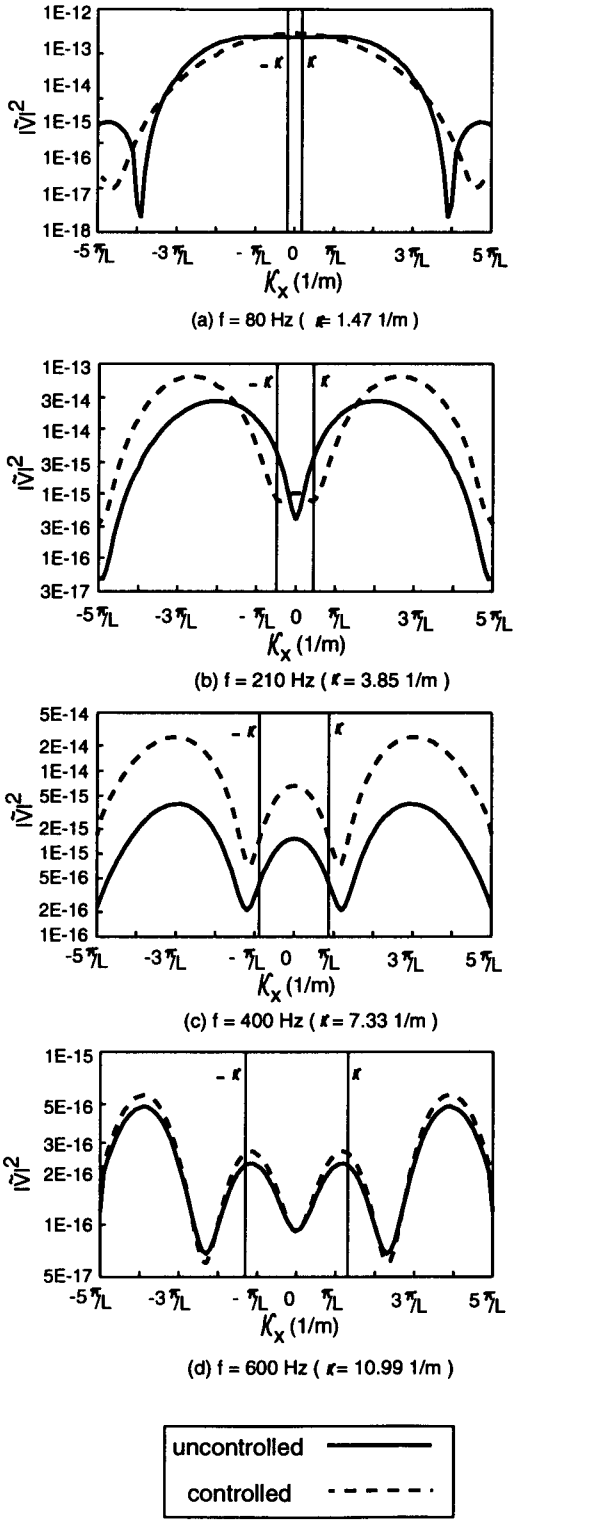

Figure 10. LMS value of velocity transform for off-resonance excitation.

solution may be to reconstruct the cost function based on the wavenumber domain sensors which can effectively reduce the supersonic wave components. In summary, this work provides a theoretical analysis for distributed types of actuators and sensors in ASAC and leads to an efficient design of an intelligent material structure system.

Table 5. Results for the off-resonance excitation cases.

excitation frequency (Hz)	reduction of Φ_w (dB)	reduction of Φ_p (dB)	control voltages (V)
80	0.6	−1.0	19.8
210	−3.3	−0.9	16.8
400	−8.0	−6.6	22.5
660	−0.5	−0.4	−10.2

Acknowledgments

The author gratefully acknowledges the support of the work by National Science Council, Republic of China, under grant NSC82-0410-E-020-001.

References

[1] Lueg, 1936 *Process of Silencing Sound Oscillator* US Patent No 2,043,416
[2] Lester H C and C R Fuller 1990 Active control of propeller induced noise fields inside a flexible cylinder *AIAA J.* **28** 1374–80
[3] Deffayet C and P A Nelson 1988 Active control of low frequency harmonic sound radiated by a finite panel *J. Acoust. Soc. Am.* **84** 2192–9
[4] Nelson P A, Curtis A R D, Elliott S J and Bullmore A J 1987 The active minimization of harmonic enclosed sound fields, Part I: theory *J. Sound Vibration* **117** 1–13
[5] Song L, Koopmann G H and Fahniline J B 1991 Active control of the acoustic radiation of a vibrating structure using a superposition formulation *J. Acoust. Soc. Am.* **89** 2786–92
[6] Jones J D and Fuller C R 1989 Active control of sound fields in elastic cylinders by multiple forces *AIAA J.* **27** 845–52
[7] Meirovitch L and Thangjitham S 1990 Control of sound radiation pressure *J. Vibration Acoustics* **112** 237–44
[8] Pan J, Hansen C H and Bies P A 1990 Active control of noise transmission through a panel into a cavity: I. Analytical study *J. Acoust. Soc. Am.* **87** 2098–108
[9] Wang B-T, Fuller C R and Dimitriadis E K 1991 Evaluation of active control of noise transmission through rectangular plates using multiple piezoelectric or point force actuators *J. Acoust. Soc. Am.* **90** 2820–30
[10] Burdisso R A and Fuller C A 1992 Dynamic behavior of structural acoustic systems in feedforward control of sound radiation *J. Acoust. Soc. Am.* **92** 277–86
[11] Dimitriadis E K, Fuller C A and Rogers C A 1991 Piezoelectric actuators for distributed vibration excitation of thin plates *J. Vibration Acoustics* **113** 100–7
[12] Wang B-T, Dimitriadis E K and Fuller C R 1991 Active control of structurally radiated noise using multiple piezoelectric actuators *AIAA J.* **29** 1802–9
[13] Fuller C R and Jones J D 1987 Influence of sensor and actuator location on the performance of active control system 87-WA/NCA-9 *ASME Annual Meeting (Boston, MA, 1987)*
[14] Clark R L and Fuller C R 1991 Control of sound radiation with adaptive structures *J. Intelligent Mater. System and Structures* **2** 431–52
[15] Clark R L and Fuller C R 1992 A model reference approach for implementing active structural acoustic control *J. Acoust. Soc. Am.* **92** 1534–44
[16] Elliott S J and Johnson M E 1993 Radiation modes and the active control of sound power *J. Acoust. Soc. Am.* **94** 2194–204
[17] Snyder S D and Tanaka N 1993 On feedforward active control of sound and vibration using vibration error signals *J. Acoust. Soc. Am.* **94** 2181–93
[18] Wang B-T and Fuller C R 1994 The effect of distributed or discrete pressure and acceleration sensors on active structural-acoustic control systems *J. Chinese Soc. Mechanical Engineers* **15** 30–9
[19] Wang B-T and Rogers C A 1991 Modeling of finite-length spatially distributed induced strain actuators for laminate beams and plates *J. Intelligent Mater. System and Structures* **2** 38–58
[20] Lee C K and Moon F C 1990 Modal sensors/actuators *J. Appl. Mech.* **57** 434–41
[21] Fahy F 1985 *Sound and Structural Vibration* (Orlando, FL: Academic)
[22] Wallace C E 1972 Radiation resistance of a baffled beam *J. Acoust. Soc. Am.* **51** 936–45
[23] Wang B-T 1992 A dynamic simulation of hybrid active and passive control of structural vibration *NSC Report* NSC81-0401-E-020-501 Republic of China
[24] Piezo Systems Inc. 1990 *Product Catalog*
[25] Pennwalt Corporation 1990 *Piezo Film Sensor Application Notes*
[26] Peng H and Lees P B 1990 Edge effect in radiation efficiency of a baffled beam below the critical frequency *J. Acoust. Soc. Am.* **88** 2001–6
[27] Clark R L, Fuller C R and Wick A 1991 Characterization of multiple piezoelectric actuators for structural excitation *J. Acoust. Soc. Am.* **90** 346–57
[28] Clark R L and Fuller C R 1992 Optimal placement of piezoelectric actuators and polyvinylidene fluoride error sensors in active structural acoustic control approaches *J. Acoust. Soc. Am.* **92** 1521–33
[29] Wang B-T, Burdisso R A and Fuller C R 1994 Optimal placement of piezoelectric actuators for active structural acoustic control *J. Intelligent Mater. System and Structures* **5** 67–77